Ultrafast excited-state isomerization in phytochrome revealed by femtosecond stimulated Raman spectroscopy

Jyotishman Dasgupta[a], Renee R. Frontiera[a], Keenan C. Taylor[b], J. Clark Lagarias[b,1], and Richard A. Mathies[a,1]

[a]Chemistry Department, University of California, Berkeley, CA 94720; and [b]Department of Molecular and Cellular Biology, University of California, Davis, CA 95616

Contributed by J. Clark Lagarias, December 2, 2008 (sent for review September 30, 2008)

Photochemical interconversion between the red-absorbing (P_r) and the far-red-absorbing (P_{fr}) forms of the photosensory protein phytochrome initiates signal transduction in bacteria and higher plants. The P_r-to-P_{fr} transition commences with a rapid *Z*-to-*E* photoisomerization at the C_{15}═C_{16} methine bridge of the bilin prosthetic group. Here, we use femtosecond stimulated Raman spectroscopy to probe the structural changes of the phycocyanobilin chromophore within phytochrome Cph1 on the ultrafast time scale. The enhanced intensity of the C_{15}–H hydrogen out-of-plane (HOOP) mode, together with the appearance of red-shifted C═C stretch and N—H in-plane rocking modes within 500 fs, reveal that initial distortion of the C_{15}═C_{16} bond occurs in the electronically excited I* intermediate. From I*, 85% of the excited population relaxes back to P_r in 3 ps, whereas the rest goes on to the Lumi-R photoproduct consistent with the 15% photochemical quantum yield. The C_{15}–H HOOP and skeletal modes evolve to a Lumi-R-like pattern after 3 ps, thereby indicating that the C_{15}═C_{16} *Z*-to-*E* isomerization occurs on the excited-state surface.

photochemistry | photoisomerization | photosensory proteins | plant signal transduction | time-resolved vibrational spectroscopy

Light sensing and signaling responses mediated by photoreceptors are critical for the survival and growth of all life forms. Phytochromes are a class of biliprotein photoreceptors found in plants, bacteria, and fungi that are capable of sensing red/far-red light via interconversion between red-absorbing (P_r) and far-red-absorbing (P_{fr}) forms (Fig. 1) (1). Light absorption by phytochrome triggers a rapid and reversible *Z*-to-*E* isomerization of the C_{15}═C_{16} methine bridge between the C and D rings of its bilin chromophore (2). This photochemistry subsequently drives changes in protein conformation that lead to changes in gene expression that influence growth and development (1, 3). Temporal resolution of the structure of the bilin chromophore during the photoisomerization process is important, not only to unravel common themes underlying ultrafast dynamics of biological reactions, but also for designing synthetic light-harvesting systems with rapid response times, efficient sensing, and energy storage.

In the past, ultrafast pump–probe electronic spectroscopy has been used to probe the excited-state dynamics of plant and cyanobacterial (Cph1) phytochromes. Such studies reveal that formation of the isomerized primary photoproduct Lumi-R, characterized by a red-shifted electronic absorption maximum at 700 nm, occurs 25–40 ps after excitation (4–10). The P_r excited state exhibits multiexponential fluorescence decay dynamics with at least two lifetimes (10 ps and 45 ps) (5), thereby implicating the presence of at least two excited states. The two-state model for P_r* decay has also received support from ultrafast transient absorption measurements on the plant phytochrome phyA, the cyanobacterial phytochrome Cph1, and the bacteriophytochrome Agp1, all of which exhibit two excited-state lifetimes characterized by a short (5–16 ps) and a long (25–40 ps) time constant (8, 10, 11). Despite the kinetic insight of these transient electronic spectroscopic studies, these techniques do not establish when the double bond isomerization occurs, nor do they resolve the molecular basis for the low P_r-to-P_{fr} photochemical quantum yields (7–16%) (12, 13).

Femtosecond mid-IR spectroscopy, a technique that probes vibrational modes in the 1,400- to 1,800-cm^{-1} window, has been used to obtain structural and temporal information during the phytochrome photoisomerization process. By using this technique, van Thor *et al.* (9) determined that the formation of Lumi-R proceeded with 3-, 14-, and 134-ps time constants, but they were unable to assign which of the three temporal phases corresponded to Lumi-R formation. A 3-ps formation time constant for the Lumi-R ground state is inconsistent with the relatively high-fluorescence quantum yield (≈0.005) and the long excited-state lifetime (≈30 ps) observed for the P_r form of plant and cyanobacterial (Cph1) phytochromes (14, 15). More recent time-resolved mid-IR work on the bacterial phytochrome Agp1 detected three time constants: 0.7 ps, consistent with the formation of the vibrationally excited ground state; 3 ps, reflecting ground-state cooling; and 33 ps, assigned to Lumi-R photoproduct formation (10). Although more consistent with previous fluorescence data, mid-IR measurements omit the structurally sensitive fingerprint region (600–1,200 cm^{-1}) and cannot easily resolve chromophore dynamics from those attributed to the overlapping protein scaffold.

Resonance Raman (RR) spectroscopy has also been used to probe selectively the ground-state chromophore structure in both P_r and P_{fr} [supporting information (SI) Figs. S1 and S2] (16, 17). In RR, photoexcitation near the electronic absorption of the chromophore resonantly enhances the chromophore modes so that the observed Raman scattering is not masked by that of the protein. Until recently, time-resolved RR had been limited to picosecond time resolution, but the recent development of femtosecond stimulated Raman spectroscopy (FSRS) has overcome this fundamental limitation (18). FSRS has the advantage of providing vibrational structural information with high temporal (≈50 fs) and spectral (≈10 cm^{-1}) resolution. This enhanced capability has been particularly revealing for structurally timing a wide variety of photochemical reactions in biomolecules (19). Here, we use FSRS to investigate the primary process of Cph1 P_r-to-P_{fr} photoconversion in the 100-fs to 100-ps time scale. These studies not only provide insight into the ultrafast structural changes associated with chromophore isomerization, but also reveal the partitioning of the excited-state product into successful and unsuccessful internal conversion pathways.

Results

The P_r ground-state stimulated Raman spectrum and transient FSRS spectra of Cph1 at selected time delays after 635-nm

Author contributions: J.D., J.C.L., and R.A.M. designed research; J.D. and R.R.F. performed research; K.C.T. and J.C.L. contributed new reagents/analytic tools; J.D., R.R.F., and R.A.M. analyzed data; and J.D., R.R.F., K.C.T., J.C.L., and R.A.M. wrote the paper.

The authors declare no conflict of interest.

[1]To whom correspondence should be addressed. E-mail: jclagarias@ucdavis.edu or ramathies@berkeley.edu.

This article contains supporting information online at www.pnas.org/cgi/content/full/0812056106/DCSupplemental.

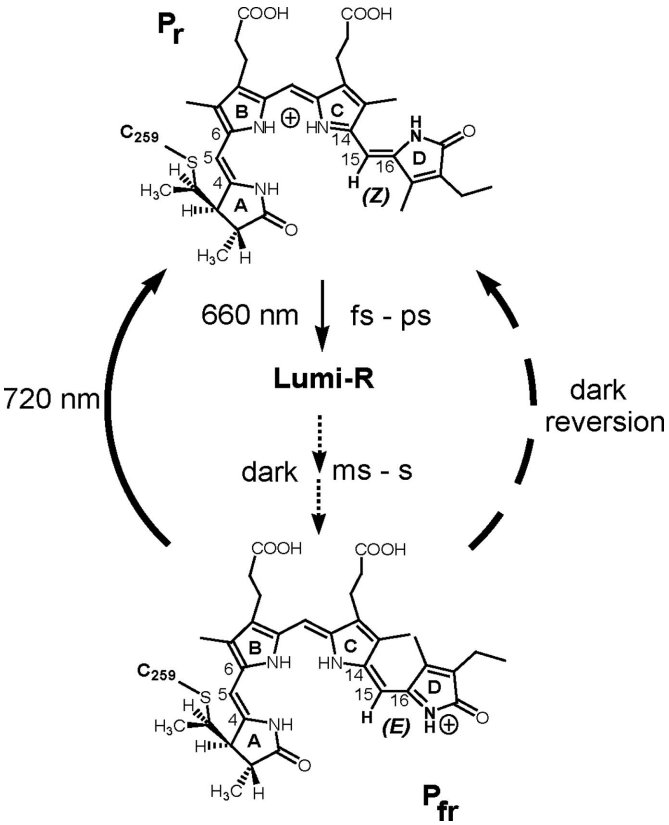

Fig. 1. Structural changes of the PCB chromophore during the P_r-to-P_{fr} photocycle in Cph1. The ground-state chromophore structure in P_r is depicted as *ZZZ*ssa at the AB, BC, and CD rings, respectively (28). Photoexcitation results in isomerization of the C_{15}═C_{16} methine-bridge between the C and D rings. The subsequent dark steps take place on the millisecond-to-second time scale to yield the red-shifted *ZZE*ssa product P_{fr}. P_r can be regenerated from P_{fr} by both far-red excitation and by a slow dark reversion process.

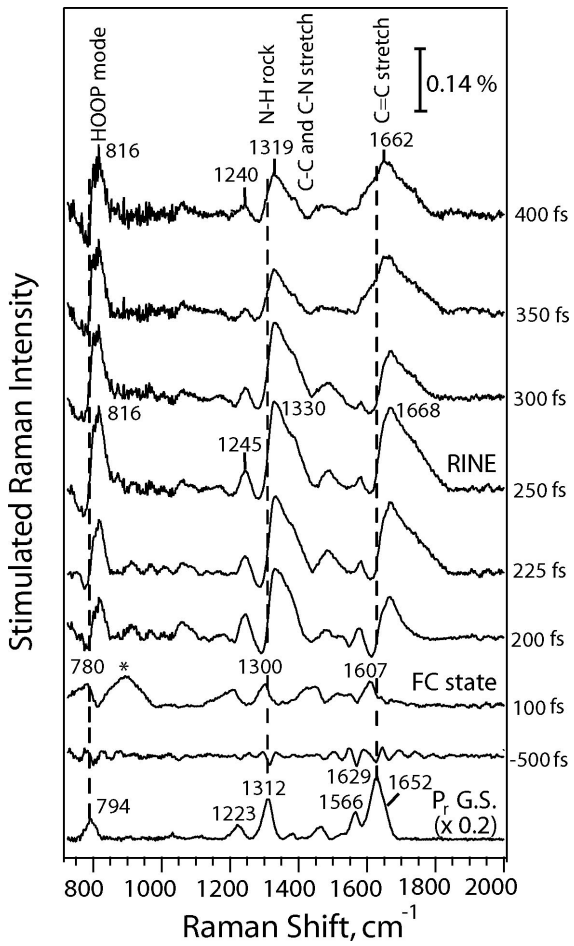

Fig. 2. Time-resolved FSRS vibrational spectra of Cph1 measured by using a 792-nm Raman pump pulse after photoexcitation of P_r at 635 nm. Dispersive peaks from 200 to 350 fs are attributed to hot luminescence features whose correspondence to the main ground-state peaks is indicated by the solid vertical lines at 794, 1,312, and 1,629 cm^{-1}. The Raman peaks from the S_1 state (after 300 fs) and the FC state (before 100 fs) are also observed. The P_r ground-state Raman spectrum is scaled by 0.2. The electronic echo artifact is marked by an asterisk.

photoexcitation are shown in Figs. 2 and 3. The ground-state spectrum exhibits dominant vibrational features at 794 cm^{-1} (vinyl C—H hydrogen out-of-plane or HOOP mode), 1,223 and 1,312 cm^{-1} (vinyl C—H and N—H in-plane rock), 1,566 cm^{-1} (in-phase in-plane N—H rock), and 1,629 cm^{-1} (C═C stretch) (20). The C═C stretch band also possesses a poorly resolved shoulder at 1,652 cm^{-1}, which, according to density functional theory (DFT) calculations (20) corresponds to the C_4═C_5 (A–B ring) stretch, whereas the main peak at 1,629 cm^{-1} represents a delocalized mode comprising the C_{15}═C_{16} methine bridge and the C_{17}═C_{18} double bond of the D ring. The medium intensity peak at 1,566 cm^{-1}, assigned to the in phase N—H in-plane rock localized to the B and C rings, reports on the protonation state of the chromophore (20). All observed vibrational frequencies are in good agreement with previous RR spectroscopy studies of Cph1 with 1,064-nm excitation (21).

The transient FSRS spectra of Cph1 from 0 to 100 fs (Fig. 2) arise from the Franck–Condon (FC) state within the experimental time resolution of 70 fs. The features at 780, 1,300, and 1,607 cm^{-1} are all red-shifted with respect to the P_r ground-state spectrum. The broad feature observed at ≈900 cm^{-1} is an artifact arising from actinic pump and probe coupling. The intensity of all three FC bands decays within 150 fs concomitant with the rise of dispersive features. These decay dynamics are in agreement with the ≈100-fs rise time of stimulated emission in transient absorption studies on Cph1 and plant phytochromes (8). Spectra from 200 to 400 fs consist of dispersive Raman features at 1,668, 1,330, 1,245, and 816 cm^{-1}, each of which correlates with a prominent P_r ground-state feature. The characteristic dispersive line shape is caused by a nonlinear effect known as Raman induced by nonlinear emission (RINE) (19), a coherent hot luminescence signal that occurs when a stimulated emission band is resonant with both the Raman pump and probe wavelengths. Although direct information about the chromophore structure is masked, the decay time of RINE features indicate how fast the stimulated emission region depopulates. The RINE intensity dynamics were quantified by the ethylenic peak amplitude that was found to decay in 320 ± 50 fs (Fig. S3).

The time-resolved FSRS spectra from 450 fs to 40 ps are presented in Fig. 3. By 450 fs, positive definite features indicative of a new region on the excited-state surface emerge, and temporal changes in these vibrational features reveal the nuclear dynamics of the chromophore. Vibrational bands at 1,609 (C═C stretch), 1,302 (D-ring N—H rock), 1,345 (C—C, C—N stretch), and 816 cm^{-1} (HOOP mode) are seen in the 600-fs spectrum that is assigned as an intermediate excited-state I*. During the 500-fs to 5-ps period, the low-frequency C═C stretch (1,609 cm^{-1}) exhibits a 5-cm^{-1} increase in peak frequency, whereas its intensity decays by 50%. After 5-ps, a small reduction in the C═C stretch intensity continues out to 40 ps. Additionally, the high-frequency C═C shoulder feature at 1,650 cm^{-1} (because of I*) red-shifts to 1,645 cm^{-1} by 40 ps. In the fingerprint region, the shoulder at 1,345 cm^{-1} in I*, which

BIOPHYSICS

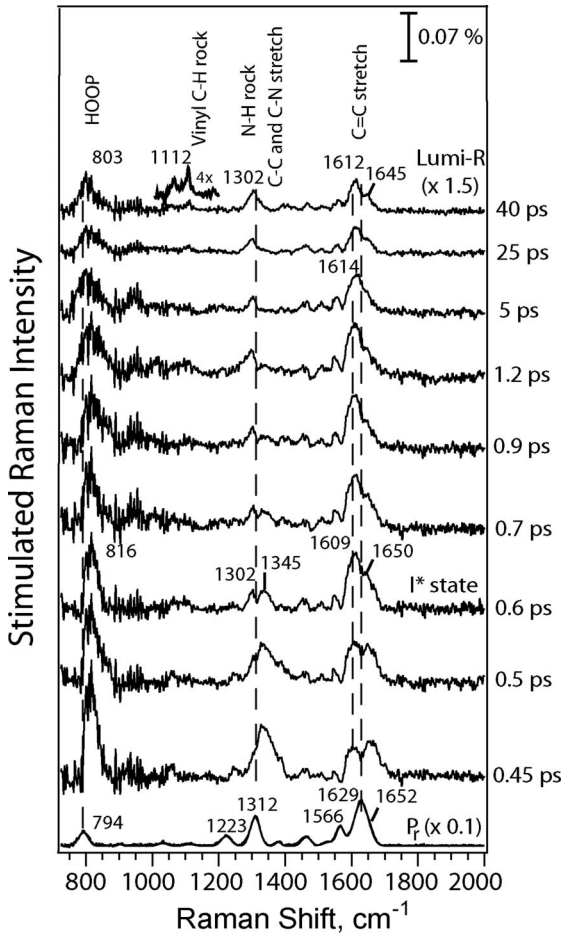

Fig. 3. Time-resolved FSRS spectra of Cph1 between 450 fs and 40 ps at selected time delays. The approximate vibrational mode description assigned to each peak has been indicated. The ground-state spectrum is scaled by 0.1. The 40-ps (Lumi-R) spectrum is blown up by 1.5.

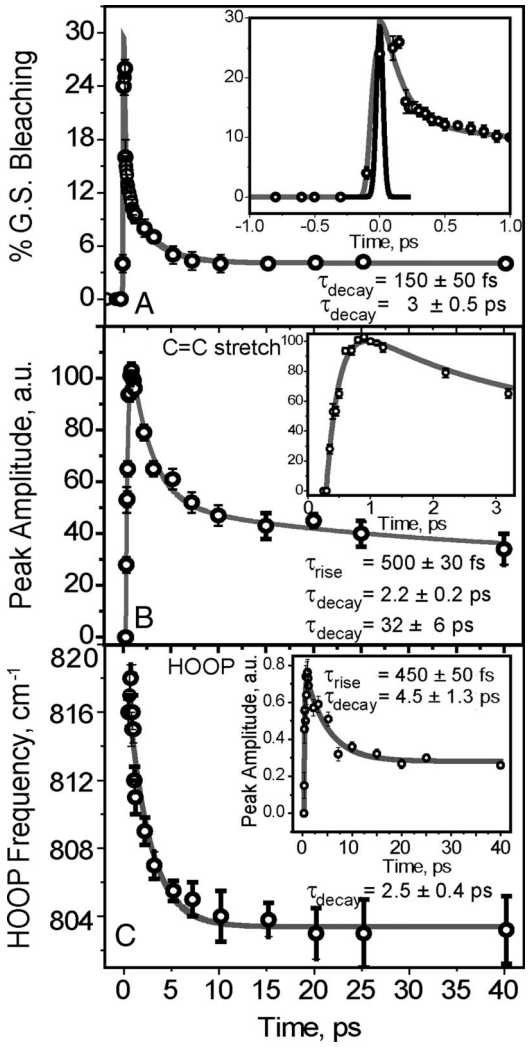

Fig. 4. Kinetic analysis of Lumi-R formation. (*A*) Ground-state recovery kinetics obtained by plotting the percentage depletion of the ground state during different delay times after photoexcitation. (*Inset*) Negative and early times in the kinetics along with the fit. The ground-state recovery is biexponential with rates: τ_1 = 150 ± 50 fs and τ_2 = 3 ± 0.5 ps. (*B*) Kinetic analysis of the Raman bands at 1,612 cm^{-1} corresponding to the C═C stretch. Open circles represent the amplitudes of the corresponding vibrational modes as a function of time delay. (*Inset*) Expands the early time region to reveal the rise time of the C═C mode. The solid line is the best fit to the experimental data. The C═C peak amplitude has three exponents: rise, τ = 500 ± 30 fs; decay, τ_1 = 2.2 ± 0.2 ps and τ_2 = 32 ± 6 ps. (*C*) Kinetic analysis of the C_{15}—H HOOP mode corresponding to the photoproduct Lumi-R. The dynamics of the HOOP peak frequency between 0.45 and 40 ps are presented. The HOOP peak frequency change is modeled to a single exponent decay with τ = 2.5 ± 0.4 ps. (*Inset*) Kinetics of the HOOP peak amplitude as a function of time. The change is modeled with two exponents: rise, τ_1 = 450 ± 50 fs; and decay, τ_2 = 4.5 ± 1.3 ps. All kinetic fits were convoluted with Gaussian instrument response function (FWHM 70 fs).

corresponds to a mixture of C—N and C—C stretch, decays with the rise of the 1,302-cm^{-1} peak (N—H in-plane rock) during the 500-fs to 25-ps time interval. A small peak at 1,112 cm^{-1} emerges at 10 ps that corresponds to the vinyl C—H rock of the Lumi-R photoproduct. The HOOP frequency also exhibits a red-shift from 816 to 803 cm^{-1} from 500 fs to 10 ps, indicating changes of the chromophore structure on the excited-state surface. At longer time delays, the intensity of the HOOP mode tapers off along with the intensity of the C═C stretching and N—H rocking modes. Additional experiments at time delays up to 100 ps confirmed that the features decrease only slightly in intensity after 40 ps (Fig. S4). All of the vibrational features seen in the temporal evolution of the FSRS signals can be directly assigned to changes of the expected vibrational modes, whereas additional bands that may indicate heterogeneity are not observed. Therefore, we expect that any alternate ground-state species is present at ≤10% of the concentration of the productive P_r species, based on the sensitivity of our apparatus with these samples.

The time scale for the *Z*-to-*E* isomerization was determined by plotting the amplitude of the RINE signals, the ground-state recovery, and the amplitude and frequencies of selected Raman bands as a function of time (Table S1). The kinetics of the RINE feature at 1,665 cm^{-1} (Fig. S3) are well fit to a convolution of our 70-fs instrument response and a single exponential decay time of 320 ± 50 fs. The ground-state recovery, quantified in Fig. 4*A* by following the depletion of the 1,629-cm^{-1} ground-state feature, exhibits two exponential phases. The first phase indicates an ultrafast (150 ± 50 fs) ground-state repopulation caused by stimulated emission, and the second is a slow recovery of ground state via internal conversion in 3 ± 0.5 ps. The longer time constant is in good agreement with the ground-state recovery kinetics measured by femtosecond mid-IR spectroscopy on Cph1 (9). The ground-state recovery dynamics show that 85% of the excited-state population reverts back to the P_r (*ZZZ*ssa) configuration by 3 ps, thereby fixing the photochemical quantum yield to 15%. Although the low photochemical quantum yield has been attributed to hetero-

geneity of the ground-state population (4), our data are more consistent with a homogeneous branching mechanism on the excited-state surface.

The kinetics of the C═C peak at 1,612 cm^{-1} (Fig. 4*B*) provide the best measure of the formation and decay of the excited state because they are unaffected by overlap with the RINE features. The peak amplitude is fit to three exponents with a 500 ± 30-fs rise time along with 2.2 ± 0.2 and 30 ± 6-ps decay components. The 500-fs exponent signifies the formation of the I* state, and the 2- to 3-ps time constant, which causes at least 50% of the C═C stretch intensity decrease, is associated with the depopulation of I*. The vibrational feature at 1,345 cm^{-1} assigned to the C—N/C—C stretching mode also decays with 3.2- and 33-ps time constants similar to the dynamics observed for the N—H in-plane rocking mode (Fig. S5). There is a marked increase in the 1,302-cm^{-1} N—H in-plane rock intensity with a 37-ps time constant. This long time constant is consistent with the decay of the excited-state absorption (ESA) at 800 nm (33 ± 2 ps) and the 26 ± 5-ps component associated with the decay of stimulated emission at longer wavelengths (840–960) nm (Fig. S6). Together, these results indicate that the ≈30-ps component represents the formation of the ground-state Lumi-R from the excited-state photoproduct (Lumi-R*).

Fig. 4*C* presents the frequency and intensity dynamics of the HOOP mode. Because HOOP intensity and frequency are correlated with out-of-plane distortions caused by steric interaction between the C and D rings, they can be used as a probe of the isomerization dynamics. The 13-cm^{-1} red-shift in HOOP frequency suggests a considerable change in the chromophore structure around the C_{15}═C_{16} bond. The peak amplitude is most intense at early times (450 ± 50-fs rise), and it relaxes with a 4.5 ± 1.3-ps time constant. The peak position of the HOOP frequency as a function of time is a probe of both the electronic changes and structural distortions of the C_{15}═C_{16} bond. The 2.5-ps time constant for the red-shift in HOOP frequency along with the 4.5-ps HOOP intensity decay are in good agreement with changes observed in the intensity of the other vibrational bands (C═C stretch and N—H rock) that cumulatively signifies the depopulation of the I* state.

Fig. 5 compares the vibrational spectra of P_r, I*, Lumi-R*, Lumi-R, and P_{fr}. In the I* spectrum, both the C═C stretch (1,609 cm^{-1}) and N—H in-plane rocking (1,302 cm^{-1}) modes are red-shifted with respect to the P_r ground-state spectrum, whereas the HOOP mode is blue-shifted to 816 cm^{-1}. The structural evolution of I* to Lumi-R* is marked by a 13-cm^{-1} red-shift of the HOOP frequency. Additionally, the unusually enhanced Raman intensity of the HOOP mode in both P_{fr} and Lumi-R indicates significant nonplanarity in the C_{15}═C_{16} bond after isomerization. However, a notable difference in the Lumi-R spectra compared with Lumi-R* is the presence of resolved vinyl C—H rock mode at 1,112 cm^{-1}. The peak frequencies and intensities for Lumi-R* and Lumi-R spectra are quite similar, and both spectra have similar intensity ratios for the three major vibrational bands, indicating that the chromophore is already isomerized in the Lumi-R* state.

Discussion

Fig. 6 presents a schematic potential energy surface summarizing the structural changes we have observed in the P_r-to-P_{fr} photoreaction of Cph1. After excitation, the system moves away from the FC region within 150 fs indicated by the rise of RINE signals (8, 11). The decay of the RINE signals marks the transition to the excited-state I* with a highly distorted chromophore structure in the C_{14}—C_{15}═C_{16} region. From the I* state, the population bifurcates with 85% relaxing back to the P_r ground state while the rest moves forward to the product-like excited-state Lumi-R*. Subsequently, the Lumi-R ground-state photoproduct is formed in 30 ps. These results will now be discussed in the framework of a molecular model in which the initial photoexcitation catalyzes an excited-state isomerization about the C_{15}═C_{16} bond that flips the D ring.

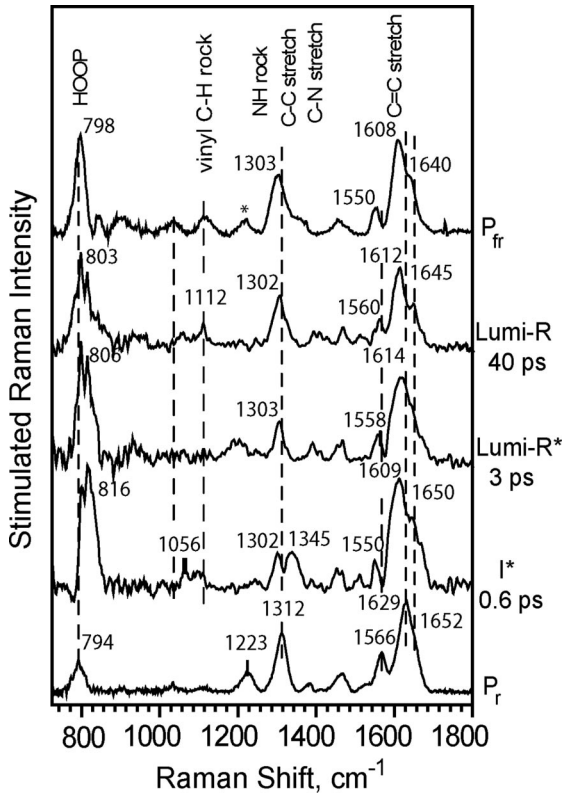

Fig. 5. Normalized FSRS spectra of P_r, I* (0.6-ps spectrum scaled by 10), Lumi-R* (3-ps spectrum scaled by 10), Lumi-R (40-ps spectrum scaled by 20), and P_{fr}. The Lumi-R, Lumi-R*, and I* spectra were smoothed by 11-point Savitzky–Golay function. The asterisk signifies a subtraction artifact.

Excited-State Dynamics of I* and Lumi-R*. The FC state vibrational features disappear within 150 fs, giving way to the RINE line shapes that mask the early evolution of the excited state. The ≈300-fs decay of the RINE features indicates when the system has evolved farther along the reaction coordinate into a new region denoted as I*. The 20-cm^{-1} red-shift of the C═C stretch mode in I* implies a charge redistribution between the C and the D rings, thereby leading to distortion at the C_{15}═C_{16} double bond. It has been shown that the N-protonated C ring in P_r is partially neutralized by a shift of electrons from the D ring that lowers the bond order of the C_{15}═C_{16} and the C_{17}═C_{18} bonds (22, 23). The resulting partial positive charge on the D ring (Fig. 1) weakens the NH in-plane rocking and C—C/C—N stretch modes (20) that are red-shifted in I* by 10 and 30 cm^{-1}, respectively. The charge redistribution should also cause the C_{14}—C_{15} bond order to increase. The out-of-plane distortion will predictably result in the intermixing of the vinyl C—H in-plane rock (1,223 cm^{-1}) with the C_{15}—H HOOP mode, thus priming the system for isomerization.

Transient changes in the C_{15}—H HOOP frequency and intensity provide an important structural probe of the isomerization reaction. DFT calculations have shown that the 794 cm^{-1} HOOP mode in the P_r spectrum arises primarily from a local C_{15}—H wag (20). Therefore, the remarkable intensity enhancement of the HOOP mode in I* signifies a dramatic increase of the out-of-plane distortion at the C_{14}—C_{15}═C_{16} moiety. The 22-cm^{-1} blue-shift of the HOOP mode along with the red-shifted vinyl C—H in-plane rock (1,056 cm^{-1} in I* vs. 1223 cm^{-1} in P_r) suggests mixing of these two modes. We believe that this C_{14}—C_{15}═C_{16} distortion initiates the low-frequency torsional motion (≈100–200 cm^{-1}) around the C_{15}═C_{16} bond. Subsequently, as the system crosses over to the Lumi-R* state, the HOOP peak position red-shifts by 13 cm^{-1}, and the C═C stretch mode is blue-shifted by 5 cm^{-1}, indicating that the

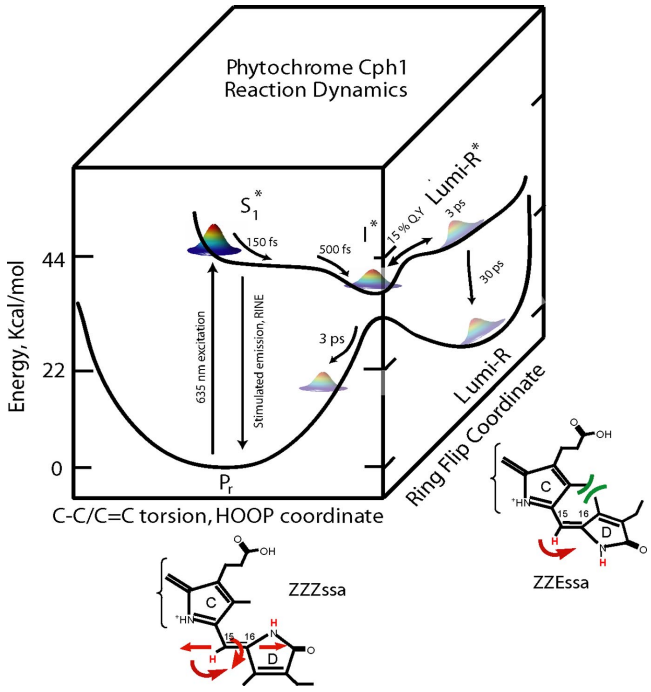

Fig. 6. Schematic potential energy surfaces involved in the Cph1 P_r-to-P_{fr} photoreaction. The system is launched on the excited-state S_1*, which has a steep initial slope in the FC region that rapidly drives the system to an excited-state intermediate I*. From I*, 85% of the population returns back to the reactant ground state while the remainder overcomes a ring-flip barrier to form a new product-like excited state. This excited state decays in 30 ps to form the Lumi-R ground state. The chemical structures of P_r and Lumi-R schematically show the modes involved during the isomerization reaction.

strain in the C_{14}—C_{15}═C_{16} moiety is relaxed. Because very few changes are observed in the FSRS spectrum after Lumi-R* formation (3–40 ps), the red-shift of the HOOP mode effectively marks the completion of the isomerization process. Thus, the excited state has two distinct regions that are in equilibrium: I*, which forms after 500 fs, having a very blue-shifted HOOP frequency; and an excited-state photoproduct Lumi-R*, which forms with a 3-ps time constant and possesses a red-shifted HOOP mode. The remarkably large frequency and intensity change of the HOOP mode during the Pr → I* ⇌ Lumi-R* conversion together with modest changes thereafter argue that photoisomerization takes place at the C_{15}═C_{16} bond and is complete on the excited-state surface in 3 ps.

The decrease in the intensity of all of the vibrational features during the I* to Lumi-R* internal conversion process reflects a loss of excited-state population caused by a barrier that redirects much of the population back to the reactant ground state (Fig. 6). This barrier is probably caused by a protein-imposed constraint on D ring rotation, thereby affecting the quantum yield. The inverse temperature dependence of P_r fluorescence has been used as an argument for the presence of a thermal barrier (≈5 kcal/mol) on the excited-state surface (24). Thus, the ≈3-ps I* decay is determined by two parallel decay pathways, one of which inefficiently (≈15%) produces Lumi-R* while the other efficiently reverts to P_r. Additionally, because the overall quantum yield of the P_r-to-P_{fr} reaction for Cph1 is ≈10–15% (13), it follows that the dark processes that take place after Lumi-R formation proceed to P_{fr} with near-unity efficiency.

Overall, the molecular mechanism can be summarized as follows. Photoexcitation reduces the π-bond order at the C_{15}═C_{16} methine bridge, thereby allowing intrinsic or nonbonded protein–chromophore interactions to induce significant distortion at the C_{14}—C_{15}═C_{16} moiety in the I* state. At this point, 15% of the I* population exploits the weakened C═C torsion potential to overcome the D ring flipping excited-state barrier yielding an isomerized Lumi-R* in 3 ps. This isomerized fraction remains on the excited state for 30 ps, at which point it decays to Lumi-R with little structural change within the chromophore. This mechanism is similar to that proposed for bacteriorhodopsin in which the *trans-cis* isomerization of the retinal is initiated by a charge transfer mechanism (25).

Kinetics of Lumi-R Formation. Small changes in the frequency and intensity of chromophore spectral features are observed between 3 and 40 ps. We attribute the 30-ps time constant associated with the peak amplitude decay of the C═C stretch, C—C/C—N stretch and the increase in N—H in-plane rock intensity to the formation of the Lumi-R ground state from Lumi-R*. The loss in intensity is likely caused by resonance de-enhancement or decrease in Raman cross-section for the relaxed Lumi-R ground-state structure. The 26-ps decay of the stimulated emission (840–960 nm) is consistent with the 28-ps excited-state lifetime attributed to the P_r* excited state from fluorescence quantum yield analysis (14). The 30-ps formation of Lumi-R is also in agreement with time-resolved transient absorption experiments on native and substituted chromophores in PhyA and Cph1 phytochromes (7, 11). Therefore, the stimulated emission decay dynamics, together with the changes in intensity of the Raman bands, directly indicate that the 3-ps *Z*-to-*E* isomerization takes place on the long-lived excited state and that the ground-state Lumi-R photoproduct forms in 30 ps.

Femtosecond mid-IR studies on Cph1 were not able to assign a specific time constant for Lumi-R formation (9), although it was indicated that the ground-state photoproduct forms by 3 ps, a time scale that is inconsistent with both our FSRS results and previous fluorescence quantum yield measurements (15). However, in a parallel study carried out on the bacteriophytochrome Agp1 by Diller and coworkers (10), the 3-ps time constant assigned to re-formation of the P_r ground state whereas a 33-ps component corresponded to the formation of the Lumi-R ground state (10). This investigation is in excellent agreement with the 3-ps ground-state recovery dynamics and 30-ps Lumi-R formation kinetics seen here.

Chromophore Structure in Lumi-R. The FSRS spectrum of the chromophore in Lumi-R* and in Lumi-R closely resembles that of P_{fr} (Fig. 5), indicating that the chromophore has completely isomerized by 3 ps. Specifically, the relative intensities of the HOOP mode to the C═C stretch in both spectra are similar. In the PCB chromophore, the intramolecular C_{13} methyl–C_{17} methyl steric interaction prevents planarity of the C_{15}═C_{16} methine bridge in the Lumi-R photoproduct and in P_{fr}. This nonplanarity is responsible for the enhanced intensity of the HOOP mode compared with the high-frequency C═C stretch in both the Lumi-R and P_{fr} states. Because the chromophore structure in Lumi-R and P_{fr} are so similar, it follows that all structural changes in the chromophore have to be confined to the primary photoisomerization step. This observation argues against the hypothesis that a single-bond rotation about C_5—C_6 takes place in the dark step subsequent to the formation of ground-state Lumi-R (17). There are, however, a few notable differences between the Lumi-R and P_{fr} spectra: the 1,560-cm^{-1} (in-phase NH rock for C and D rings) band in Lumi-R is blue-shifted by 10 cm^{-1} whereas the HOOP mode is blue shifted by 5 cm^{-1} compared with the P_{fr} state. These small differences in peak frequency position in P_{fr} and Lumi-R likely arise from changes in H bonding and/or charge redistribution to the bilin C and D rings occurring in the dark steps subsequent to the photoisomerization that are responsible for the pronounced red-shift of the P_{fr} form (1, 23).

Overall, our data corroborate the hypothesis that there are two distinct regions on the excited state that are in equilibrium as proposed by Holzwarth and coworkers (5). They argued that a

thermal equilibrium exists between the initially excited state of P_r phytochrome (i.e., I*) and a conformationally relaxed, although still electronically excited intermediate state that we assign to Lumi-R* (Fig. 6). The barrier in the excited state shows this eventual transition along the HOOP and ring flip coordinate. Thus, the major structural changes take place on the excited-state state surface, and the isomerization occurs with the 3-ps transition from I* to Lumi-R*.

Conclusions

Time-resolved structural studies have been used to clarify the kinetics of the P_r-to-P_{fr} photoisomerization process and to determine the molecular structural details of when and how the isomerization occurs. By using femtosecond time-resolved Raman, we identify the time scale of formation for the primary photoproduct Lumi-R and assign the key vibrational modes that are involved in the photochemistry. After excitation, the system evolves on the multidimensional excited-state surface leading to the formation of the intermediate I* in 500 fs, which is significantly distorted along the C_{14}—C_{15}═C_{16} moiety. A fraction (15%) of this distorted population goes on to form Lumi-R* via the D ring flipping over an excited-state barrier. The majority is unable to complete the ring flip and internally converts back to ground-state P_r. Subsequently, the remaining Lumi-R* relaxes to the Lumi-R ground state in 30 ps. Thus, the low-photochemical quantum yield is caused by branching during the internal conversion of I* on the excited-state surface. The enhanced intensity and altered frequency of the C_{15}—H HOOP mode directly argue that the isomerization takes place at the C_{15}═C_{16} bond and is complete on the excited-state surface by 3 ps.

Materials and Methods

Protein Samples. Recombinant Cph1(N514) was expressed and purified as a phycocyanobilin-bound holoprotein as described and detailed in *SI Materials and Methods* (26). Samples were concentrated to 11 OD_{656} per cm followed by overnight dialysis against 1 L of buffer [25 mM Tes-KOH (pH 8.0), 25 mM KCl, 10% glycerol] before spectroscopic studies.

Spectroscopic Measurements. The FSRS setup has been described in detail in ref. 18. A home-built mode-locked Ti:sapphire oscillator seeds a 1-kHz, 800-μJ regenerative amplifier (Alpha 1000/US; BMI) yielding 50-fs pulses centered at 795 nm. The laser fundamental was split into three pulses necessary for FSRS. One portion of the fundamental was used to drive a noncollinear optical parametric amplifier thereby generating a broadband 635-nm [full width at half-maximum (FWHM) $\approx$800 cm^{-1}] actinic pump pulse (400 nJ, compressed to 30 fs) to initiate P_r-to-P_{fr} photochemistry. At 635 nm, the optical density of the sample was $\approx$0.85 OD per mm (see Fig. S1), and the actinic pump power of 400 nJ ($\approx$50-μm beam diameter) resulted in 26% ground-state depletion (27). A 3.5-ps narrow bandwidth Raman pulse (792 nm, 1.7–2 μJ) was created by passing a second portion of the laser fundamental through a grating filter. The probe pulse was produced by continuum generation of a third portion of the fundamental passed through a 3-mm-thick sapphire plate, followed by pulse compression in a fused-silica prism compressor ($\approx$20 fs, 12 nJ). The near-IR portion of the continuum was selected with an 830-nm long-pass filter that was split into probe and reference beams by a 50:50 beam splitter, producing a 6-nJ probe pulse at the sample point to produce a spectrum extending from 830 to 960 nm.

The three FSRS pulses were focused through the transverse 1-mm pathlength of a homemade 1 × 2 × 40-mm Borofloat-glass flow channel. The 500-μL sample stored in a glass reservoir was driven through the flow cell by a peristaltic pump connected with PTFE (0.5-mm inner diameter) tubing. All measurements were performed at room temperature. The flow rate ($\approx$1 mL min^{-1}) was adjusted to replenish fresh sample for each laser pulse, thereby allowing sufficient time for photoexcited material to be photoconverted back to P_r ground state before reentry to the sample flow cell. This was accomplished by irradiation of the reservoir by two high-power LEDs (720 nm, 5 mW, 30° viewing angle Roithner Lasertechnik) through a RG695 long-pass filter (Newport, Inc.). Sample integrity was confirmed by both steady-state Raman and UV/visible spectroscopy before and after the experiments; no irreversible spectral changes were observed.

The FSRS spectrum was determined as the ratio of the Raman pump-on probe spectrum divided by the Raman pump-off probe spectrum after normalization with the reference. The presented time-resolved spectra are the average of 600 alternating 60-ms Raman pump-on and Raman pump-off probe exposures, producing a total acquisition time of 72-s per time point. The instrument spectral resolution was $\approx$18 cm^{-1} as determined by the FWHM of the cyclohexane 802-cm^{-1} peak. The temporal instrument response is a Gaussian, with a FWHM of 70 fs as measured by the optical Kerr effect. The $t = 0$ time delay was initially set by the cross-correlation but was allowed to vary freely in the fitting of the ground-state reconversion kinetics. To reveal the changes in the vibrational features at each time delay, we subtract a scaled ground-state spectrum from each of the excited-state FSRS spectra (see Fig. S2). The scale factor, indicative of the contribution of the residual ground-state population and its repopulation, was determined by the intensities of the 1,629- and 1,312-cm^{-1} ground-state Raman bands. All of the kinetics were fit to two- or three-exponent models with instrument response time deconvolution.

ACKNOWLEDGMENTS. We thank Dan Wandschneider, Mark Creelman, and Dr. Nathan C. Rockwell for helpful suggestions. This work was supported by the Mathies Royalty Fund and by National Institutes of Health Grant GM068552 (to J.C.L.).

1. Rockwell NC, Su YS, Lagarias JC (2006) Phytochrome structure and signaling mechanisms. *Annu Rev Plant Biol* 57:837–858.
2. Gärtner W, Braslavsky SE (2003) The phytochromes: Spectroscopy and function. *Photoreceptors and Light Signalling*, ed Batschauer A (Royal Soc Chemistry, Cambridge, UK), pp 136–180.
3. Jiao Y, Lau OS, Deng XW (2007) Light-regulated transcriptional networks in higher plants. *Nat Rev Genet* 8:217–230.
4. Kandori H, Yoshihara K, Tokutomi S (1992) Primary process of phytochrome: Initial step of photomorphogenesis in green plants. *J Am Chem Soc* 114:10958–10959.
5. Holzwarth AR, Venuti E, Braslavsky SE, Schaffner K (1992) The phototransformation process in phytochrome. 1. Ultrafast fluorescence component and kinetic models for the initial $P_r \rightarrow P_{fr}$ transformation steps in native phytochrome. *Biochim Biophys Acta* 1140:59–68.
6. Savikhin S, Wells T, Song PS, Struve WS (1993) Ultrafast pump–probe spectroscopy of native etiolated oat phytochrome. *Biochemistry* 32:7512–7518.
7. Bischoff M, Hermann G, Rentsch S, Strehlow D (2001) First steps in the phytochrome phototransformation: A comparative femtosecond study on the forward ($P_r \rightarrow P_{fr}$) and back reaction ($P_{fr} \rightarrow P_r$). *Biochemistry* 40:181–186.
8. Heyne K, *et al.* (2002) Ultrafast dynamics of phytochrome from the cyanobacterium *Synechocystis*, reconstituted with phycocyanobilin and phycoerythrobilin. *Biophys J* 82:1004–1016.
9. van Thor JJ, Ronayne KL, Towrie M (2007) Formation of the early photoproduct Lumi-R of cyanobacterial phytochrome Cph1 observed by ultrafast midinfrared spectroscopy. *J Am Chem Soc* 129:126–132.
10. Schumann C, Gross R, Michael N, Lamparter T, Diller R (2007) Subpicosecond midinfrared spectroscopy of phytochrome Agp1 from *Agrobacterium tumefaciens*. *Chemphyschem* 8:1657–1663.
11. Müller MG, Lindner I, Martin I, Gärtner W, Holzwarth AR (2008) Femtosecond kinetics of photoconversion of the higher plant photoreceptor phytochrome carrying native and modified chromophores. *Biophys J* 94:4370–4382.
12. Kelly JM, Lagarias JC (1985) Photochemistry of 124-kilodalton *Avena* phytochrome under constant illumination in vitro. *Biochemistry* 24 6003–6010.
13. Lamparter T, *et al.* (1997) Characterization of recombinant phytochrome from the cyanobacterium *Synechocystis*. *Proc Natl Acad Sci USA* 94:11792–11797.
14. Fischer AJ, Lagarias JC (2004) Harnessing phytochrome's glowing potential. *Proc Natl Acad Sci USA* 101:17334–17339.
15. Andel F, Hasson KC, Gai F, Anfinrud PA, Mathies RA (1997) Femtosecond time-resolved spectroscopy of the primary photochemistry of phytochrome. *Biospectroscopy* 3:421–433.
16. Fodor SPA, Lagarias JC, Mathies RA (1990) Resonance Raman analysis of the P_r and P_{fr} forms of phytochrome. *Biochemistry* 29:11141–11146.
17. Mroginski MA, Murgida DH, Hildebrant P (2007) The chromophore structural changes during the photocycle of phytochrome: A combined resonance Raman and quantum chemical approach. *Acc Chem Res* 40:258–266.
18. McCamant DW, Kukura P, Yoon S, Mathies RA (2004) Femtosecond broadband-stimulated Raman spectroscopy: Apparatus and methods. *Rev Sci Inst* 75:4971–4980.
19. Kukura P, McCamant DW, Mathies RA (2007) Femtosecond stimulated Raman spectroscopy. *Annu Rev Phys Chem* 58:461–488.
20. Andel F, *et al.* (2000) Probing the photoreaction mechanism of phytochrome through analysis of resonance Raman vibrational spectra of recombinant analogues. *Biochemistry* 39:2667–2676.
21. Remberg A, *et al.* (1997) Raman spectroscopic and light-induced kinetic characterization of a recombinant phytochrome of the cyanobacterium *Synechocystis*. *Biochemistry* 36:13389–13395.
22. Borg OA, Durbeej B (2007) Relative ground and excited-state pK_a values of phytochromobilin in the photoactivation of phytochrome: A computational study. *J Phys Chem B* 111:11554–11565.
23. Rohmer T, *et al.* (2008) Light-induced chromophore activity and signal transduction in phytochromes observed by ^{13}C and ^{15}N magic-angle spinning NMR. *Proc Natl Acad Sci USA* 105:15229–15234.
24. Sineshchekov VA (1995) Photobiophysics and photobiochemistry of the heterogeneous phytochrome system. *Biochim Biophys Acta* 1228:125–164.
25. Schenkl S, van Mourik F, van der Zwan G, Haacke S, Chergui M (2005) Probing the ultrafast charge translocation of photoexcited retinal in bacteriorhodopsin. *Science* 309:917–920.
26. Gambetta GA, Lagarias JC (2001) Genetic engineering of phytochrome biosynthesis in bacteria. *Proc Natl Acad Sci USA* 98:10566–10571.
27. Mathies R, Oseroff AR, Stryer L (1976) Rapid-flow resonance Raman spectroscopy of photolabile molecules: Rhodopsin and isorhodopsin. *Proc Natl Acad Sci USA* 73:1–5.
28. Essen L-O, Mailliet J, Hughes J (2008) The structure of a complete phytochrome sensory module in the P_r ground state. *Proc Natl Acad Sci USA* 105:14709–14714.